

# Journal of Semiconductors

JOS

iopscience.iop.org/jos  
www.jos.ac.cn

## Towards electronic-photonic-converged thermo-optic feedback tuning

Min Tan, Kaixuan Ye, Da Ming, Yuhang Wang, Zhicheng Wang, Li Jin, and Junbo Feng

Citation: M Tan, K X Ye, D Ming, Y H Wang, Z C Wang, L Jin, and J B Feng, Towards electronic-photonic-converged thermo-optic feedback tuning[J]. *J. Semicond.*, 2021, 42(2).

View online: <https://doi.org/10.1088/1674-4926/42/2/023104>

## Articles you may be interested in

[Ultra-wide tuning single channel filter based on one-dimensional photonic crystal with an air cavity](#)

Journal of Semiconductors. 2017, 38(2), 023004 <https://doi.org/10.1088/1674-4926/38/2/023004>

[Precision photonic integration for future large-scale photonic integrated circuits](#)

Journal of Semiconductors. 2019, 40(5), 050301 <https://doi.org/10.1088/1674-4926/40/5/050301>

[Silicon-graphene photonic devices](#)

Journal of Semiconductors. 2018, 39(6), 061009 <https://doi.org/10.1088/1674-4926/39/6/061009>

[Emerging technologies in Si active photonics](#)

Journal of Semiconductors. 2018, 39(6), 061001 <https://doi.org/10.1088/1674-4926/39/6/061001>

[Ultralow-power polymer electro-optic integrated modulators](#)

Journal of Semiconductors. 2019, 40(7), 070401 <https://doi.org/10.1088/1674-4926/40/7/070401>

[Silicon photonic transceivers for application in data centers](#)

Journal of Semiconductors. 2020, 41(10), 101301 <https://doi.org/10.1088/1674-4926/41/10/101301>



Follow JOS WeChat public account for more information

# Towards electronic-photonic-converged thermo-optic feedback tuning

Min Tan<sup>1,2,†</sup>, Kaixuan Ye<sup>1</sup>, Da Ming<sup>1</sup>, Yuhang Wang<sup>1</sup>, Zhicheng Wang<sup>1</sup>, Li Jin<sup>3</sup>, and Junbo Feng<sup>3</sup>

<sup>1</sup>School of Electronic and Optical Information, Huazhong University of Science and Technology, Wuhan 430074, China

<sup>2</sup>Wuhan National Laboratory of Optoelectronics, Huazhong University of Science and Technology, Wuhan 430074, China

<sup>3</sup>United Microelectronics Center, Chongqing 400030, China

**Abstract:** As Moore's law approaching its end, electronics is hitting its power, bandwidth, and capacity limits. Photonics is able to overcome the performance limits of electronics but lacks practical photonic register and flexible control. Combining electronics and photonics provides the best of both worlds and is widely regarded as an important post-Moore's direction. For stability and dynamic operations considerations, feedback tuning of photonic devices is required. For silicon photonics, the thermo-optic effect is the most frequently used tuning mechanism due to the advantages of high efficiency and low loss. However, it brings new design requirements, creating new design challenges. Emerging applications, such as optical phased array, optical switches, and optical neural networks, employ a large number of photonic devices, making PCB tuning solutions no longer suitable. Electronic-photonic-converged solutions with compact footprints will play an important role in system scalability. In this paper, we present a unified model for thermo-optic feedback tuning that can be specialized to different applications, review its recent advances, and discuss its future trends.

**Key words:** power management IC; integrated photonics; electronic-photonic convergence; thermo-optic tuning; feedback

**Citation:** M Tan, K X Ye, D Ming, Y H Wang, Z C Wang, L Jin, and J B Feng, Towards electronic-photonic-converged thermo-optic feedback tuning[J]. *J. Semicond.*, 2021, 42(2), 023104. <http://doi.org/10.1088/1674-4926/42/2/023104>

## 1. Introduction

Due to both physical and economic limits, Moore's law is approaching its end. Meanwhile, new applications are emerging rapidly, raising energy efficiency, capacity, and data rate challenges. Many post-Moore's directions are proposed to address the above challenges. Integrated photonics is among the most promising ones, as it offers the benefits of high data rate, low transmission loss, wide spectrum range, etc. Integrated photonics, especially silicon photonics, has made tremendous progress in the past few years. By leveraging the microelectronics fabrication platform, large-scale device fabrication and integration is made possible with silicon photonics.

Nevertheless, integrated photonics lacks practical photonic registers and flexible control and needs to be combined with electronics for any practical purpose. Integrated photonic devices suffer from many uncertainties, such as fabrication errors, supply voltage changes, and temperature variations. In many situations, these uncertainties prevent the devices from reliable operations.

Feedback tuning is an effective approach to maintain reliable operations of these photonic devices. For example, the resonant wavelength of a micro-ring is strongly affected by the process and temperature variations, and a feedback stabilization loop is required to fix the wavelength. For dynamic operations, a feedback mechanism is also required to ensure that the photonic devices are operating at the desired operat-

ing point. For example, we monitor the status of optical switches and set it to the expected operating state. Thus, for both stability and dynamic operations considerations, feedback photonic parameter tuning is required. Many tuning mechanisms have been proposed in the literature. The thermo-optic effect is among the most frequently used ones due to the advantages of high efficiency and low loss. Up to now, most thermo-optic feedback tuning solutions use PCB-level or benchtop solutions. These conventional solutions are no longer suitable for large-scale integration, and the convergence of electronics and photonics is an irresistible trend<sup>[1]</sup> and is listed as one of the ten grand engineering challenges of 2020 by the China Association for Science and Technology. Electronic integrated circuits (EIC) focuses on the interaction between electrons and electrons, and photonic integrated circuits (PIC) focuses on the interaction between light and matter. As shown in Fig. 1(a), electronic-photonic convergence (EPC) includes electronics and photonics as key ingredients but focuses more on the interaction between electrons and photons. As shown in the design hierarchy [Fig. 1(b)<sup>[2]</sup>], EPC is moving to the next design hierarchy, that is, electronic-photonic heterogeneously-converging integrated circuits.

The remainder of this paper is organized as follows. Section 2 proposes a unified model for thermo-optic feedback tuning and discusses its design challenges. Section 3 focuses on each building blocks. Section 4 reviews the state-of-the-art designs. Section 5 points out future trends. Section 6 concludes this paper.

## 2. Unified model and challenges

Fig. 2 shows the unified model for the design and analysis

Correspondence to: M Tan, [mtan@hust.edu.cn](mailto:mtan@hust.edu.cn)

Received 19 NOVEMBER 2020; Revised 28 DECEMBER 2020.

©2021 Chinese Institute of Electronics

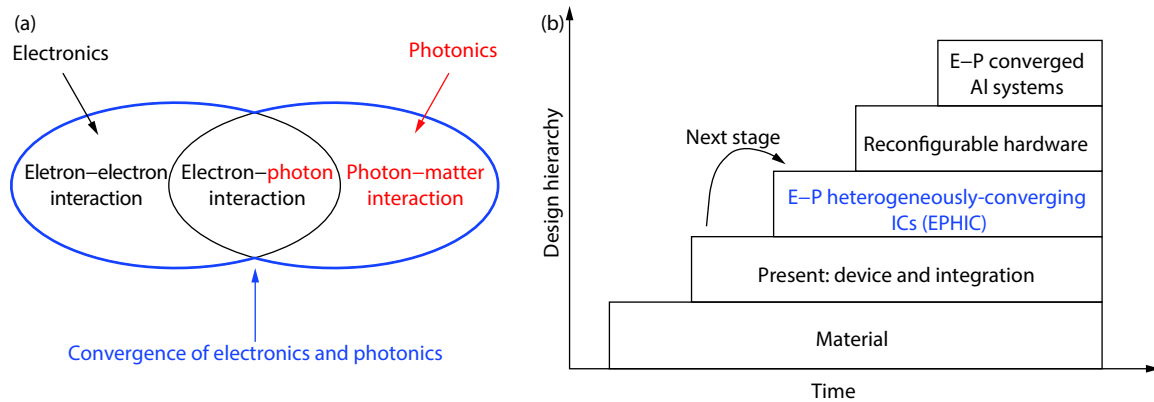


Fig. 1. (Color online) (a) The convergence of electronics and photonics. (b) Design hierarchy of electronic-photon convergence<sup>[2]</sup>.

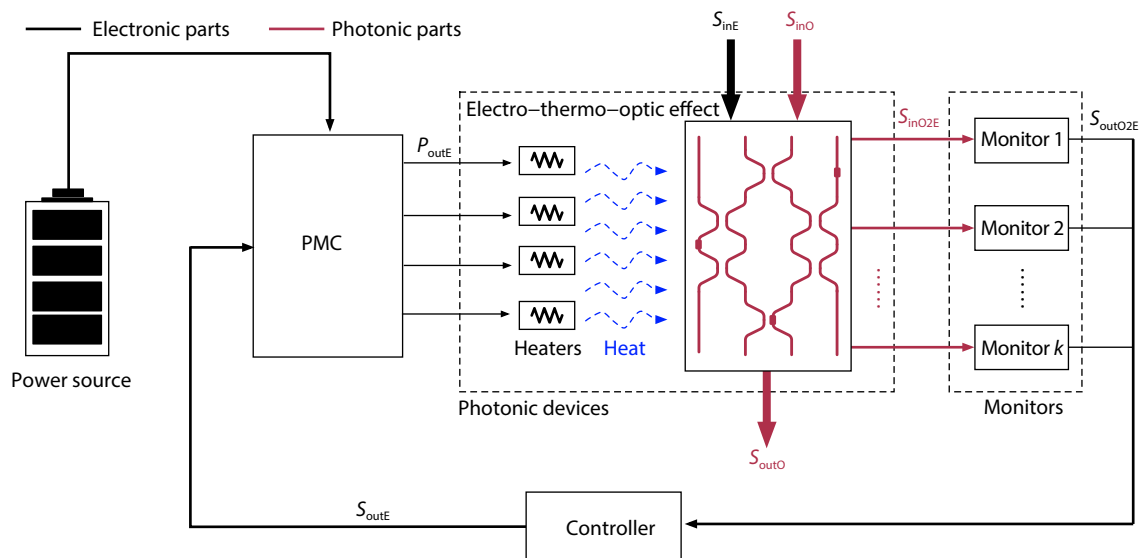


Fig. 2. (Color online) The unified model of a thermo-optic feedback tuning system.

is of a thermo-optic feedback tuning system. The photonic part consists of one or multiple devices, possibly with multiple photonic inputs and multiple photonic outputs. Furthermore, it may have multiple open-loop electronic input signals and multiple closed-loop electronic input signals. The monitors obtain the status information of the photonic devices, e.g., the wavelength of a micro-ring resonator, beam-forming direction of an optical phased array (OPA), etc. After processing the monitoring information, the controller passes the processed signal to a power management circuit (PMC) for thermo-optical tuning.

There are multiple challenges for thermo-optic feedback tuning. From the microelectronics industry's experiences, to cope with the increasing design complexity, compact device modeling and design automation tools need to be developed. Also, we need to develop cost-efficient, reliable, and efficient monitoring techniques. Furthermore, a low-power and compact controller is required. Compared with conventional power converters for electronics, thermo-optic tuning has a different power and voltage ranges, loading conditions, and bandwidth requirements and brings new design challenges and opportunities. Many applications, such as optical phased array and optical switches, requires a large number of heaters, and scalability is the key challenge. For the thermo-op-

tic phase shifter (TOPS), it is quite challenging to reduce its power consumption while achieving a wide bandwidth. TOPS has been used in many applications, such as the wavelength tuning of micro-ring modulators, bias tuning of Mach-Zehnder modulators, polarization control, optical neural network (ONN)<sup>[3]</sup>, optical phased array (OPA)<sup>[4]</sup>, and silicon quantum photonic circuits<sup>[5]</sup>. Different applications have different performance requirements and deserve different design considerations.

### 3. Building blocks

The performance of thermo-optic feedback tuning critically depends on that of its building blocks. So far, most building blocks use PCB or benchtop solutions and very few of them adopted integrated solutions. In this section, we discuss the research progress of each building block.

#### 3.1. Thermo-optic phase shifting

A typical thermo-optic phase shifter (TOPS) consists of a waveguide and a heater (a purely resistive load). The heat generated by the heater diffuses to the waveguide and changes its refractive index. Putting the heater closer to the waveguide reduces the diffusing time but increases the optical loss. Vice versa, putting the heater farther from the wave-

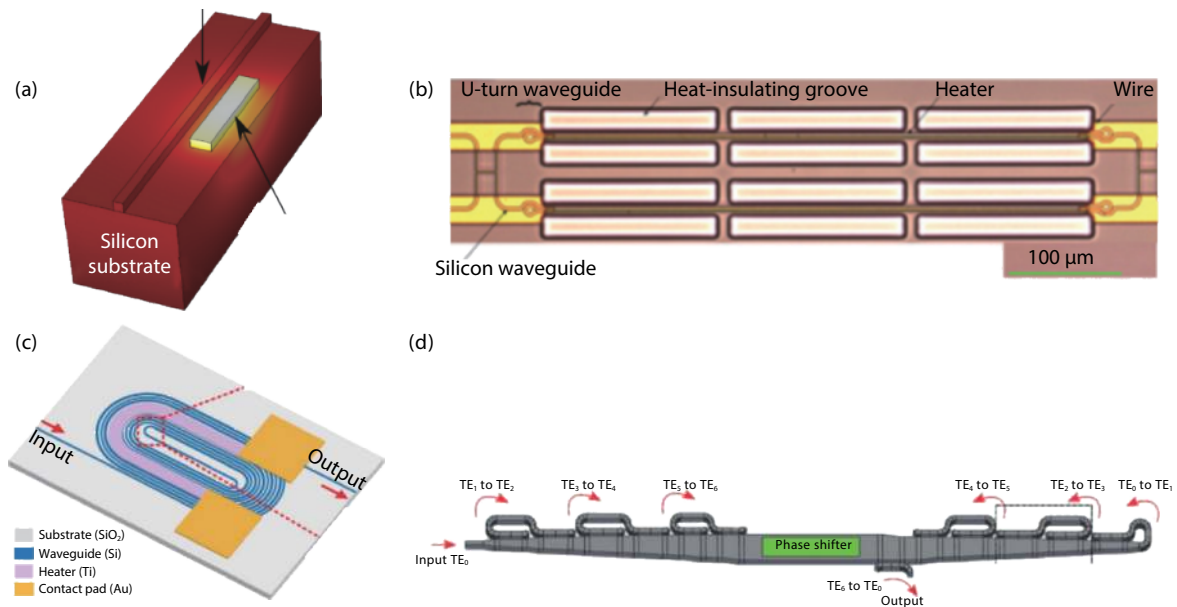


Fig. 3. (Color online) TOPS structures of (a) conventional<sup>[6]</sup>, (b) air-trench<sup>[7]</sup>, (c) multi-bend<sup>[8]</sup>, and (d) multi-pass<sup>[9]</sup>.

Table 1. Summary of TOPS designs.

Ref.	Undercut	Heater	P <sub>π</sub> (mW)	Size (μm <sup>2</sup> )	Bandwidth (kHz)	Loss (dB)	Resistance (Ω)
[7]	Yes	TiN	0.4	500 × 20	0.2	0.55	–
[8]	No	Ti	3.0	67 × 28	39	0.9	–
[9]	No	Metal	1.7	880 × 365	53.8	6	–
[13]	No	TiN	2.56	109 × 21	10.1	1.23	249.5
[14]	No	TiN	21.4	320 × 2.5	62.5	<0.4	540
	No	N++Si	22.8	320 × 2.0	159	<0.4	1100

guide reduces the optical loss but results in more power consumption and reduced bandwidth. The performance of a TOPS depends on its material and structure. There are tradeoffs in TOPS designs, and different techniques have been proposed to optimize the TOPS performances.

The conventional structure is shown in Fig. 3(a)<sup>[6]</sup> with the heater sitting beside the waveguide. There is a cladding between the waveguide and the heater. However, some heat would be wasted on the cladding, reducing the heating efficiency. To improve the heating efficiency, Refs. [10–12] remove the cladding material and directly integrates the heater within the waveguide. Another popular approach is to isolate the waveguide from the substrate with an air trench, as shown in Fig. 3(b)<sup>[7]</sup>. However, this approach slows down the heat diffusion. Both techniques are susceptible to mechanic stress and require complicated fabrication processes. Another option is to apply the multi-bend structure, as shown in Fig. 3(c)<sup>[8, 13]</sup>. This structure can recollect the wasted heat in the cladding. Consequently, it has better heating efficiency. The heat can transfer into the substrate quickly, achieving much higher bandwidth than the air-trench structure. However, the bend radius has to be carefully designed to reduce optical loss. Another option is to apply the multi-pass structure, as shown in Fig. 3(d)<sup>[9]</sup>. The light phase is tuned every time it passes the heated area, and the heating efficiency is enhanced by the number of passes with little additional loss. Table 1 lists the performances of the state-of-the-art TOPS designs. Each TOPS is relatively small, ranging from tens of μm<sup>2</sup> to a few thousand μm<sup>2</sup>. The required output

power is only about tens of mW. The typical bandwidth of the TOPS is around tens of kHz.

The thermo-optic performance also depends on the materials of the waveguide and the heater. SOI waveguide has high absorption in some spectral bands, e.g., 532–900 nm wavelength window<sup>[9, 13, 14]</sup>. Silicon nitride (SiN) waveguide has a broad transparent window with low scattering loss<sup>[15–18]</sup>, but its thermo-optic (TO) coefficient is relatively low. Polymer waveguide has a large TO coefficient, fast response time, high flexibility, and low fabrication cost, but has poor reliability<sup>[19, 20]</sup>. The heater is usually made of metal or semiconductor. A metal heater is usually put above the waveguide; the semiconductor heater usually sits aside the waveguide. Heaters of different materials have different resistivities. For the same physical size and tuning efficiency, the metal heater has much lower resistance and V<sub>π</sub> than those of the semiconductor heater<sup>[21]</sup>.

### 3.2. Power management circuit (PMC)

Most TOPS designs apply PCB or benchtop power supplies. These solutions are not practical for large-scale integrated systems, and an integrated power supply is the key to achieve a compact footprint. Low-dropout (LDO) regulator is the preferred power supply, especially for supplying many heaters, as it can be fully integrated and has a compact chip area and accurate output voltage with a small ripple. So far, power management circuit (PMC) specific to thermal-tuning is still in its early development stage. Different from conventional LDO applications, thermo-optical tuning has different re-

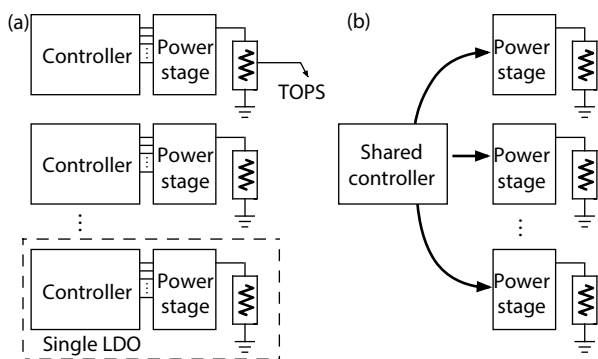


Fig. 4. Block diagrams of (a) multiple LDOs and (b) a TDM LDO that drives multiple TOPS.

quirements. To support a large temperature tuning range, a large output range is required. To reduce the unwanted heat generation, a high efficiency is required. For fast thermo-optic tuning, a wide bandwidth is required. To enable high scalability, a small chip area is required. The required power for each TOPS is in the range of tens of mWs. Consequently, the power stage of the LDO is much smaller than conventional applications. To reduce the chip area, Ref. [22] proposed to share the controller between different channels with the time-division multiplexing (TDM) scheme. Fig. 4 shows the comparison between the conventional way and the TDM LDO to drive multiple TOPSs. As each TOPS's required tuning power is relatively small, the controller occupies a large percent of the total chip area. Sharing the controller saves the total chip area and improves system scalability.

There are two popular methods to control the LDO: the output of a DAC<sup>[4]</sup> and the pulse width modulation (PWM) signal<sup>[23, 24]</sup>. Fig. 4 shows the diagrams of these two driving schemes. The DAC generates a reference signal for the LDO, while the PWM method modulates the duty ratio of the LDO's conducting time. The DAC approach is shown in Fig. 5(a); the efficiency depends on the actual dropout voltage. Fig. 5(b) shows the PWM approach. Due to the low-pass filtering nature of the TOPS, the local temperature of the TOPS is constant for a fixed duty ratio<sup>[23]</sup>. We can tune the temperature by modulating the duty ratio of the PWM signal. The efficiency of the PWM depends on the minimum achievable dropout voltage. The PWM approach usually has better efficiency than the DAC approach. The accuracy of the PWM approach depends on not only the TOPS bandwidth but the duty ratio and the frequency of the PWM signal. According to calculation<sup>[23]</sup>, for 150 kHz TOPS, the PWM signal should be as high as 8 MHz to keep the relative output ripple below 0.01.

### 3.3. Monitor

The monitor senses the operating state of the photonic devices. Various techniques have been proposed in the literature: (1) on-chip photodetectors (PDs) to monitor the light intensity at the output ports<sup>[25–30]</sup>; (2) on-chip temperature sensor<sup>[31–33]</sup>; (3) in-resonator photoconductive heaters (IRPHs) to monitor the light intensity in the waveguide<sup>[34–36]</sup>; (4) Contact less integrated photonic probe (CLIPP) to measure the light-intensity-dependent change of waveguide's electrical conductivity<sup>[37–39]</sup>.

On-chip PDs are the most commonly used monitoring method, but they need to tap a portion of light from the optic-

al path. This increases the insertion loss and makes it not suitable for applications with many tapping points. The on-chip temperature sensor has a negligible loss but cannot determine the state of the device without knowing its initial state. It generally needs to be combined with PD-based initial state monitoring to compensate for the process deviations and environmental thermal fluctuations. IRPHs are formed by doped waveguide, as Fig. 6(a) shown. The doping sections allow the IRPH to be used as a doped resistive heater and also provide a means of photodetection due to defect state absorption<sup>[34]</sup>. This solution has negligible loss too. The feedback loop based on this method could well compensate for temperature changes and process deviations. Still, a lot of pre-calibration work is required to determine the device characteristics. For example, the dark current changes with different heating voltages, and every IRPHs must be calibrated to obtain the device transmission, as shown in Figs. 6(b) and 6(c). This makes it difficult to be used in large-scale applications. The CLIPP places two metal electrodes on top of the waveguide, as shown in Fig. 7, and monitors variations of the waveguide electric conductance  $\Delta G$  that are induced by a carrier generation effect<sup>[39]</sup>. This solution introduces negligible loss, but the readout circuits are too complicated.

### 3.4. Controller

So far, most controllers in thermo-optic feedback tuning are implemented using board-level circuits, especially those with multiple photonic devices<sup>[26, 29, 30, 40–42]</sup>. A few recent designs with a single photonic device have integrated controllers<sup>[43–47]</sup>.

For single photonic device applications, there are some basic algorithms, e.g., dithering<sup>[48]</sup>, locking to maximum or minimum<sup>[26, 29]</sup>, locking to reference<sup>[44, 45, 47, 49]</sup>, and so on. In the dithering approach, a small dithering signal is applied thermally to the device, resulting in a small modulation of the output optical signal. The dithering component of the output signal indicates the operating state of the photonic devices. Locking to maximum or minimum algorithm is also called the hill-climbing algorithm. It perturbs the operating state of the device and determines if the current operating point needs a positive change or a negative change<sup>[30]</sup>. It is limited to applications with a global peak or valley. Locking to reference needs an external reference<sup>[49]</sup> or self-reference<sup>[44, 45, 47]</sup>. The external reference is manually added, and the self-reference can be achieved via a lookup table<sup>[50]</sup> or a reference point generated by the controller internally<sup>[44, 45, 47]</sup>. Depending on the difference between monitoring value and reference value, the controller determines if the device's current operating point needs a positive change or a negative change.

For applications with multiple photonic devices, most designs use a single controller to serve a single photonic device<sup>[40, 41]</sup>. Few designs multiplex the controllers to reduce area. If all devices share one controller, each device's tuning speed will be reduced because the tuning of one device has to wait until the tuning of all other devices is finished. In Ref. [51], a pipelined time-division-multiplexing (PTDM) scheme is proposed that takes advantage of the speed mismatch between heater ( $\sim 100 \mu\text{s}$ ) and controller ( $\sim \mu\text{s}$ ). The controller tunes other devices before processing the first device's heater is finished, as shown in Fig. 8. Note that there is no

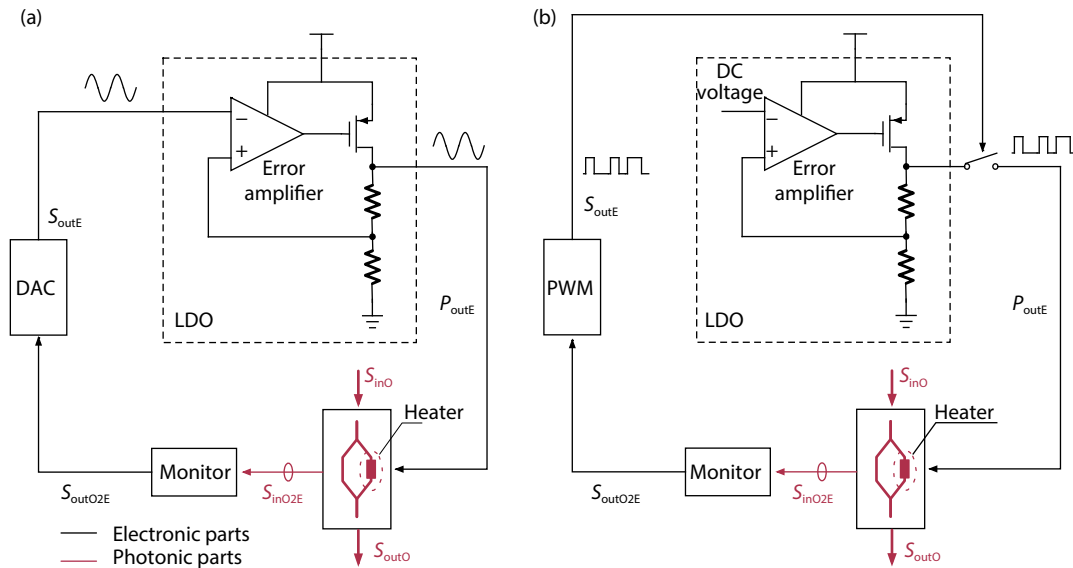


Fig. 5. Driving the TOPS with (a) DAC and (b) PWM generator.

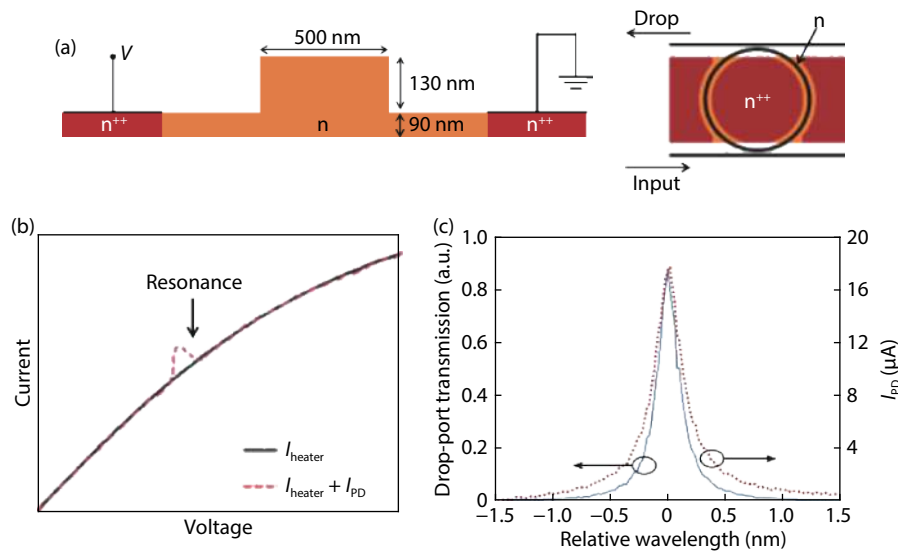


Fig. 6. (Color online) (a) Cross-section of a photoconductive n-doped silicon waveguide and its integration into a ring resonator to form an IRPH. (b)  $I$ - $V$  characteristics of an IRPH with the input laser turned off and on. (c) Calibrated drop-port transmission and photocurrent of a single ring resonator filter relative to its resonance wavelength<sup>[35]</sup>.

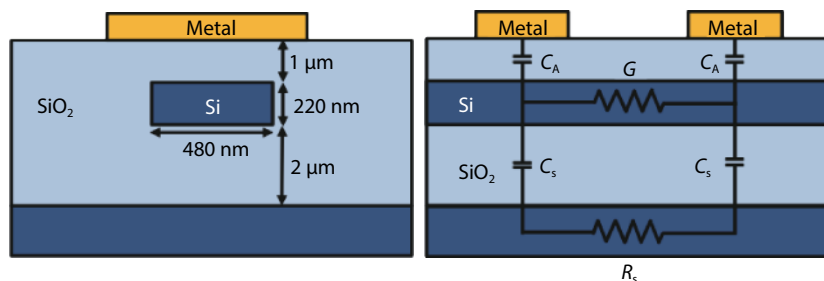


Fig. 7. (Color online) Left: Cross-section of the Si core waveguide, with the CLIPP electrode deposited on top of the SiO<sub>2</sub> cladding. Right: Longitudinal profile of the Si waveguide showing the CLIPP equivalent circuit in the electrical domain<sup>[39]</sup>.

speed degradation in the PTDM scheme. This scheme reduces the chip size significantly without sacrificing the tuning speed. It can potentially be extended to hundreds of photonic devices, pointing out a way towards large-scale electronic-photonic convergence.

#### 4. State-of-the-art designs

The proposed unified model is specialized to different applications, including wavelength control of micro-ring (MR) filters, wavelength locking of MR modulators, bias control and

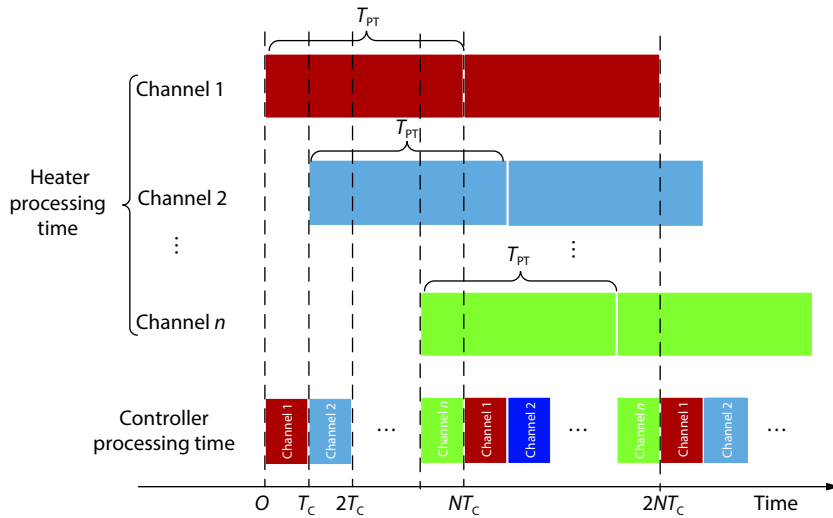


Fig. 8. (Color online) Operating principle of a pipelined TDM scheme<sup>[51]</sup>.

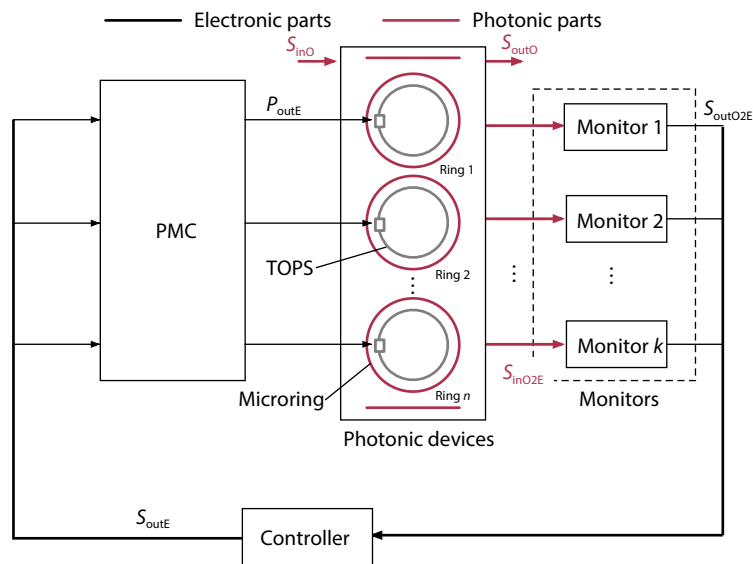


Fig. 9. (Color online) The general model for thermo-optic feedback wavelength control of a high-order MR filter.

feedback polarization control of Mach-Zehnder modulators, and optical phased arrays. Most existing designs are board-level solutions, and very few designs implemented the controller on-chip. The co-design of related building blocks enables us to achieve better performance than optimizing each building block independently. Eventually, all electronic and photonic blocks will be merged together to form the electronic-photonic-converged thermo-optic feedback tuning.

**4.1. Wavelength control of MR filters**

The MR can be used as a filter, and MR filters have small area and low power consumption. However, the resonant wavelength of the MR filter is sensitive to thermal fluctuations, input laser fluctuations and process deviations. Thermal-optic feedback control loop is an effective method for this challenge. Compared with single MR filters, high-order MR filters have better performance in terms of roll-off, pass-band flatness, and extinction ratio. Most high-order MR filters are manually tuned to achieve a flat and wide passband. Few designs could realize automatic wavelength locking. Fig. 9 shows the block diagram for thermo-optic feedback tuning

of MR filters. On the basis of every MR's resonance state obtained by monitors, the controller optimizes the filter's transmission by PMICs tuning each TOPS inside the MR.

In Ref. [52], the board-level controller obtains as input the drop port's optical power of the high-order MR filter and controls the wavelength of each MR by automatically tuning the heater of each MR one by one to maximize the drop port's optical power. This scheme may exist much iteration time and convergence problems. In Refs. [34, 35], the proposed scheme performs automatic configuration and wavelength locking of each MR. It uses IRPHs to simultaneously monitor and tune the resonance of each MR. Each MR is tuned one by one through a feedback loop composed of digital-to-analog converters (ADCs), computers, and analog-to-digital converters (DACs). After multiple iterations, the alignment of the resonant wavelengths of all MRs is achieved. Given the distance between each MR ranges from tens of nanometers to hundreds of nanometers, there is strong thermal crosstalk between adjacent MRs. The thermal crosstalk will increase the number of iterations of the controller. In Ref. [53],

Table 2. Summary of wavelength control of MR filters.

Ref.	Monitor	Controller	PMC	TOPS	Photonic device	Integration method
[52]	Photodiode	Lock to Max.	PCB solution	Doping heater	5-order MR filter	PCB
[34, 35]	IRPHs	Lock to Ref.	PCB solution	Doping heater	4-order MR filter	PCB/Computer
[54]	Photodiode	Lock to Min.	PCB solution	Metal heater	3-order MR filter	PCB
[55]	Photodiode	Lock to Max.	PWM	Doping heater	Single MR filter	Monolithic

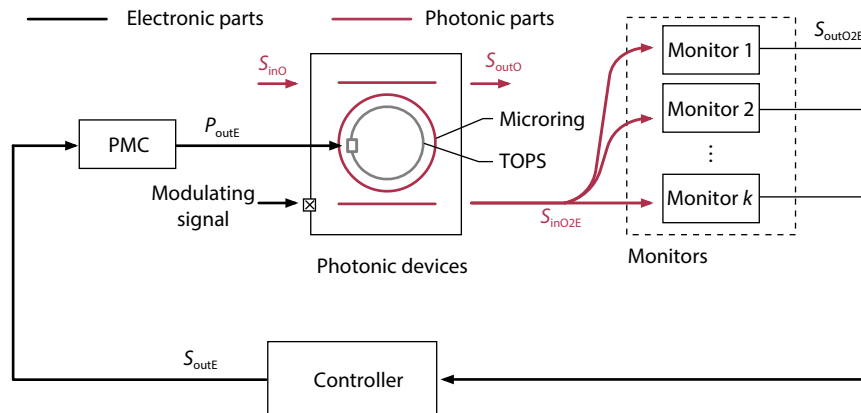


Fig. 10. (Color online) The general model for thermo-optic feedback wavelength locking of an MR modulator.

Table 3. Summary of wavelength locking of a Si MR Modulator.

Ref.	Monitor	Controller	PMC	TOPS	Photonic device	Integration method
[45]	Photodiode	Lock to Ref./Average power detection	DAC	Doping heater	Depletion MRM	Wire-bonding
[56]	Photodiode	Lock to Ref./Average power detection	PCB solution	Metal heater	Depletion MRM	Off-chip
[28]	Photodiode	Lock to Max./OMA maximum	DAC	Metal heater	Depletion MRM	Flip-chip
[46]	Photodiode	Lock to Ref./Eye maximum	DAC	c-Si heater	Depletion MRM	Monolithic
[33]	Photodiode/Temperature sensor	Lock to Ref./OMA maximum	DAC	Doping heater	Depletion MRM	Monolithic
[57]	Photodiode	Lock to Ref./OMA maximum	Power DAC	Metal heater	Depletion MRM	Cu-pillar 3D integration

a thermal eigenmode decomposition (TED) method that reduces the number of iterations of MR adjustment is proposed. However, when the number of MRR increases, it requires that each MR's heater be adjusted at the same time, making the controller more complicated and not suitable for large-scale integration. In Ref. [55], a monolithic PWM-driven closed-loop wavelength locking circuit for MRR is proposed to achieve better energy efficiency than linear driver. But the performance of closed-loop PWM control scheme, such as stability, accuracy and speed, should be further considered carefully. Table 2 summarized the automatic wavelength locking designs of high order MR filter.

#### 4.2. Wavelength locking of Si MR modulators

Silicon micro-ring modulators (MRMs) have a small size, high modulation bandwidth, and low power consumption. Nevertheless, the MRM's resonant wavelength ( $\lambda_0$ ) is sensitive to thermal, input laser, and process variations. The closed-loop wavelength locking is an effective method to address the challenge. Fig. 10 shows the general model for thermo-optic feedback stabilization of a micro-ring modulator. The monitors acquire the information related to the optical signal from the MRM and outputs the electrical signal to the controller.

The controller calculates the output value through an appropriate locking algorithm. Finally, the integrated heater is driven by a PMC to tune the resonant wavelength of MRM to the optimal point.

In Refs. [45, 56], changes in the mean power of the modulated-signal can be used to detect shifts in the temperature of the microring modulator. But it may not work efficiently when non-dc balanced data sequence is transmitted or the power of input laser has changed. In Ref. [28], a maximum OMA locking algorithm is proposed, but manual delay adjustment and a specific data transmission sequence are required. The bit-statistical<sup>[46]</sup> method can be used to achieve wavelength locking of an MRM when transmitting random data sequences. This work is the first monolithic integrated MRM transceiver with a closed-loop wavelength control circuit. However, a specific training data sequence is also required to make the tracker work correctly. Furthermore, extra delay control between the counter and the integrating front-end is necessary. In Ref. [33], the MRM's temperature is monitored by a temperature sensor, and then its resonant wavelength is tuned properly with an integrated heater. However, a high-speed optical modulation amplitude (OMA) monitor is required for the temperature sensor to determine

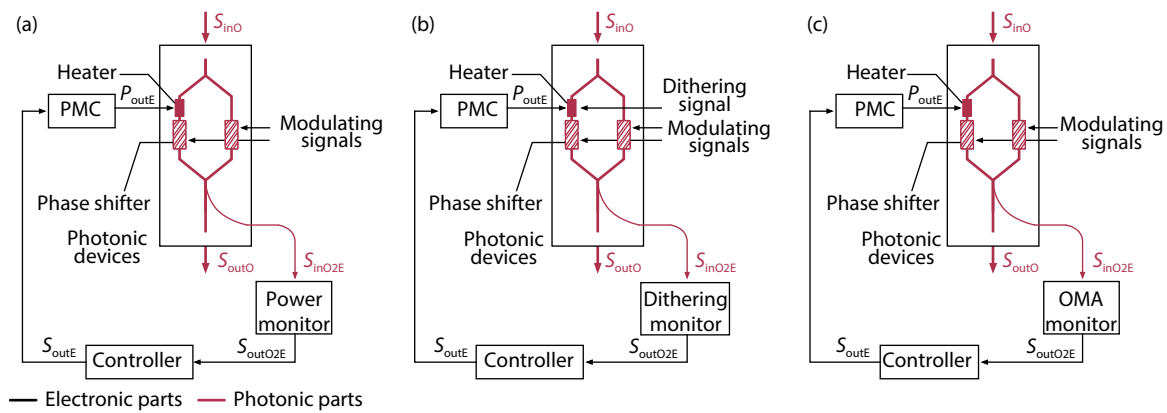


Fig. 11. Bias control schemes. (a) Output/power monitor method. (b) Dithering method. (c) OMA monitor methods.

Table 4. Summary of bias control schemes.

Ref.	Monitor	Controller	PMC	TOPS	Photonic device	Integration method
[63]	Photodiode (power detection)	Lock to Ref	PCB solution	–	LiNbO <sub>3</sub> MZM	Computer
[64]	Photodiode (power detection)	Lock to Ref	PCB solution	–	LiNbO <sub>3</sub> MZM	PCB
[50, 65]	Photodiode (dithering detection)	Lock to Ref	PCB solution	–	LiNbO <sub>3</sub> MZM	Computer
[62]	Photodiode (dithering detection)	Lock to Ref	PCB solution	Metal heater	Silicon MZM	PCB
[66]	Photodiode (OMA detection)	Max search	Charge pump	–	LiNbO <sub>3</sub> MZM	Integrated controller
[67]	Photodiode OMA + power detection)	Max search and PID control	DAC	–	LiNbO <sub>3</sub> MZM	Integrated controller

the relationship between the maximum OMA and the temperature, resulting in a high-power consumption. Ref. [57] reports a 112 Gb/s MRM with a high-speed driver and an average-power-based thermal control immune to input laser power fluctuations. However, for non-DC-balanced NRZ data, this method may fail unless it cooperates with bit-statistics in the data or conditioning the sensor front-end with transmitting data<sup>[58]</sup>. The precoding scheme<sup>[59]</sup> achieves automatic wavelength locking of MRM by precoding the transmission data. This scheme does not require a specific data sequence and works well with random data transmission sequences. Related works are summarized in Table 3.

### 4.3. Feedback bias control

Mach-Zehnder modulator is a widely used high-speed electro-optic modulator. However, the bias point of an MZM will drift over time due to various factors (e.g., temperature change). This bias point drift is independent of materials, be it lithium niobite (LiNbO<sub>3</sub>), gallium arsenide (GaAs), indium phosphide (InP), or silicon, and greatly affects the MZM performance<sup>[60, 61]</sup>. By adjusting the phase shifters on the arms of the MZM through closed-loop bias control, the bias drift can be canceled out.

Most of the existing works are designed for LiNbO<sub>3</sub> MZM. Very few works are targeted at silicon MZM<sup>[62]</sup>, but discrete devices are used. Due to the large thermo-optic coefficient of silicon, TOPSS with high efficiency and compact footprint are used to set the bias point of an MZM<sup>[75]</sup>. Integrated bias controller is the key to large-scale electronic-photonic convergence and is under active investigation.

Various bias control schemes have been proposed and

can be classified into three types depending on the bias drift extraction methods: output power monitoring method<sup>[63, 64]</sup>, dithering method (or pilot tone method)<sup>[50, 62, 65]</sup>, and optical modulation amplitude (OMA) monitoring method<sup>[66, 67]</sup>. The general models of these bias control schemes are shown in Fig. 11. A portion of the output light is coupled to the monitor. The controller then adjusts the relative phase difference of the two arms through PMC and heater according to the monitor information. Thus, a bias feedback control loop is formed. Fig. 11(a) shows the model when specialized the output power monitoring method. This method uses the output optical power or the derivative of output optical power to determine the current bias point. Different output optical power or different derivative of output optical power corresponds to the different bias points. By building a look-up table, it is easy to identify the current bias point based on the output optical power and compensate for the bias point drift with a phase shifter<sup>[63, 64]</sup>. Fig. 11(b) shows the model when specialized to the dithering method. This method makes use of the differences in nonlinearities at different operating points of the MZM transfer function. At different bias points, the transfer function of the MZM has different nonlinearities. By monitoring the harmonic components generated by the dithering signal, the current bias point can be extracted. Furthermore, to eliminate the influence of the input optical power fluctuation, the ratio between the second-order harmonic component and the fundamental component, which is independent of input optical power, can also be used to identify the current bias point<sup>[50]</sup>. Then the controller adjusts the phase shift accordingly. Fig. 11(c) shows the model when specialized to the OMA monitoring method. This method monitors the optic-

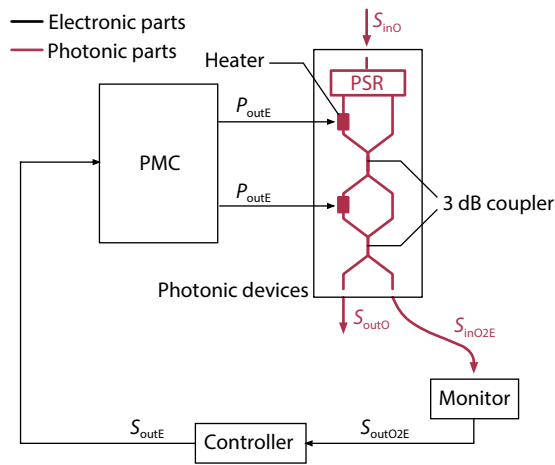


Fig. 12. The general model for feedback polarization control.

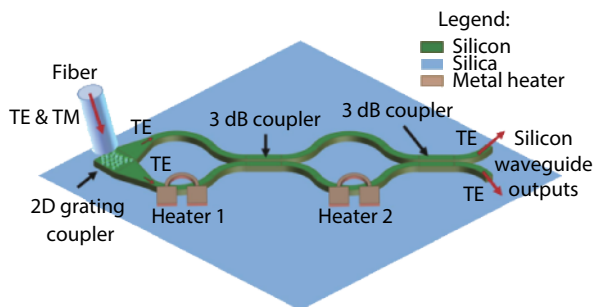


Fig. 13. (Color online) The proof-of-concept prototype in Ref. [69].

al modulation amplitude from the output while modulating the signal with fixed amplitude. If the MZM is biased at the quadrature point, the OMA reaches the maximum. Vice versa, the OMA reaches the minimum if the MZM is biased at peak point or null point. Thus, the current bias point can be defined by the current OMA and the feedback bias point stabilization is achieved. Besides, the OMA monitor method can be combined with the output power monitor method to reduce the power consumption<sup>[67]</sup>. By utilizing the OMA monitor method with max search control algorithm to find the optimal bias point and lock it by output power monitor method with PID control algorithm, the power efficient bias control scheme can be achieved. Related works are summarized in Table 4.

#### 4.4. Feedback polarization control

The polarization of light cannot maintain during the propagation in the fiber due to various factors such as temperature change, external stress, and fabrication error, resulting in the unstable and time-varying polarization state at the output of the fiber. Photonic devices are polarization-sensitive since its effective refractive index depends on the polarization states. The polarization mismatch between the SMF and the PIC will strongly reduce the signal quality. There are two main approaches to eliminate the polarization mismatch problem. One method is called polarization diversity<sup>[68]</sup>. This method requires two identical photonic integrated circuits for independent processing of different polarizations, resulting in large chip area. The other one is active polarization control (Fig. 12). In this method, the 2DGC<sup>[69, 70]</sup> or edge coupler with the PSR<sup>[71–74]</sup> is used to couple and convert the light's horizontally and vertically polarized components into two quasi-TE modes. Then the two modes are sent to a combiner that con-

sists of two phase-shifters and two 3-dB couplers. The combiner compensates the magnitude mismatch and phase mismatch between the two modes and combine them into one output port of the combiner. The other output port of the combiner is used for monitoring. For an input with a dynamical polarization state, the relative phase shift to achieve magnitude and phase compensation is time-varying, and feedback control is required for real-time adjustment. For silicon photonics, thermo-optic phase shifters are used to achieve real-time phase adjustment. Current polarization control solutions cannot meet the demand of large-scale integration. Integrated polarization controller is the key to large-scale electronic-photon convergence and is under active investigation.

A proof-of-concept prototype is demonstrated in Ref. [69], and manual control is adopted to verify the concept (Fig. 13). The real-time polarization control is successfully implemented in Ref. [71] by the greedy linear descent (GLD) control algorithm. In Ref. [70], the active polarization control scheme is used in the WDM link and successfully adapts four channels into a standard Si photonic integrated circuit with stable output power. In Ref. [72], active polarization control is applied to the coherent detection to automatically adjust and align the polarization state of each signal light with that of the LO light. In Ref. [73], the different control algorithm used in active polarization control is analyzed, verified, and compared. Furthermore, the active polarization control can be combined with the wavelength control of micro-ring filters to achieve a tunable WDM polarization-independent receiver<sup>[74]</sup> (Fig. 14). Related works are summarized in Table 5.

#### 4.5. Optical phased array

Optical phased array (OPA) is one of the key components in a light detection and ranging (LiDAR) system for optical beam forming and steering. It consists of an array of antenna elements that are controlled by phase shifters. The phase difference between two adjacent antenna elements is  $\Delta\phi$ . When the optical path delay in one direction cancels out with the phase difference, the optical beam forms in a certain direction. Most OPAs operate in the open-loop mode, i.e., the control signals are directly generated from the given register files or lookup tables. However, for practical operation, the OPA should be calibrated for external influences e.g., temperatures, process variations, etc. Consequently, it should operate in the closed-loop mode. Fig. 15 shows the general model of the closed-loop OPA.

To obtain high resolution and fast speed, hundreds even thousands of phase shifters are normally required in an OPA<sup>[4, 76–79]</sup>. TOPS is a great candidate for phase shifting in OPAs for its compact size and small power consumption. Each TOPS in the OPA should be controlled by the electronics independently. Most designs only integrate the photonic devices, and electronic parts are realized in a PCB board<sup>[78]</sup>. However, it occupies a large chip area and significantly limits the scalability of the system. To reduce the total chip area, Ref. [76] integrates the electronic drivers and the photonic devices separately. In Refs. [4, 79], the electronic and photonic parts are integrated monolithically in a single chip. Ref. [77] realize the OPA with a 3D integration process. Related works are summarized in Table 6.

Owing to process variation, every OPA demands calibration after fabricating and packaging. In addition, the OPA

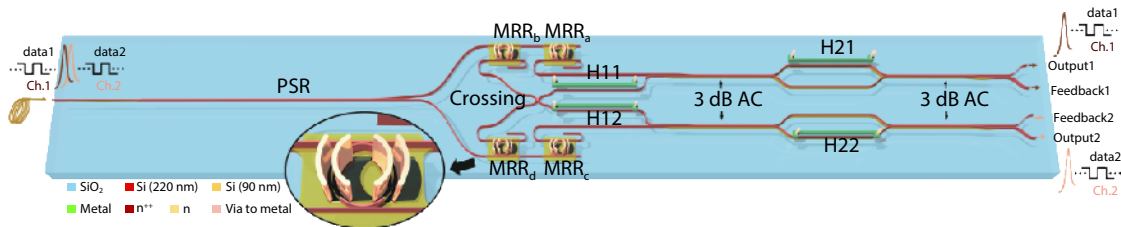


Fig. 14. (Color online) A tunable WDM polarization-independent receiver with active polarization control<sup>[74]</sup>.

Table 5. Summary of feedback polarization control schemes.

Ref.	Monitor	Controller	PMC	TOPS	Photonic device	Integration method
[69]	Powermeter	Manual	–	Metal heater	2DGC/3 dB coupler	–
[71]	Photodiode	Min search	PCB solution	Metal heater	Edge coupler/PSR/TOPS/3 dB coupler/PD	Computer
[70]	Photodiode	Min search <sup>1</sup>	PCB solution	–	2DGC/GC/OTPS/MMI/PD	Computer
[73]	Photodiode	Min search <sup>2</sup>	PCB solution	Metal heater	Edge coupler/TOPS/PSR/3 dB asymmetric coupler/PD	Computer
[74]	Photodiode	Min search <sup>3</sup>	PCB solution	Metal heater	Edge coupler/TOPS/PSR/3 dB coupler/Micro-ring/Crossing/PD	Computer

1. GLD control algorithm. 2. Two-point step size gradient descent-based and two-stage optimization method-based control algorithms. 3. Two-point step size gradient descent-based control algorithms.

Table 6. Summary of the optical phased arrays.

Ref.	Monitor	Controller	PMC	TOPS	Photonic device	Integration method
[4]	Powermeter	–	DAC	Metal heater	Grating coupler optical antenna	Monolithic
[76]	IR camera	–	PWM driver	Doping heater	Grating coupler optical antenna	Integrated drivers
[77]	Photodetector	–	DAC	Doping heater	Apodized grating antenna	3D Integrated
[78]	IR camera	–	PCB solution	Metal heater	Grating coupler optical antenna	PCB
[79]	Photodetector	–	DAC	Doping heater	Grating coupler optical antenna	Monolithic
[81]	IR CCD	Gradient-search algorithm	–	Doping heater	Emitter	–
[82]	IR CCD	Interference technique	–	–	Grating coupler optical antenna	–
[83]	Photodetector	DSGD <sup>2</sup>	DAC	–	Emitter	–

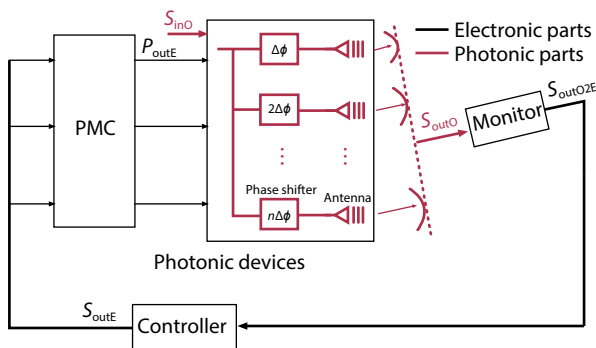


Fig. 15. The general model for the closed-loop optical phased array.

should be calibrated at every steering angle. The calibration efficiency will impact its manufacturing cost and practical applications. Many calibration algorithms are proposed in the literature<sup>[80–83]</sup>. Ref. [80] presents a modified rotating element electric field vector method to calibrate the initial condition. Ref. [81] applies the gradient-search algorithm for initial calibration. In Ref. [82], it presents an interference-based calibration method that is physical and has lower requirements on feedback systems. Ref. [83] presents a deterministic stochastic gradient descent (DSGD) method that allows calibration in microsecond timescales. Each calibration algorithm owns its advantages and disadvantages with different time spent. Currently, the convergence rate of the algorithm and the transmis-

sion rate of the interface cannot meet the requirements for mass production based on the existing methods and systems. An improved algorithm, combining the forms of multiple methods, should be developed. Besides, as the OPA currently depends on the hard-to-get far-field pattern for calibration, mapping the far-field pattern to on-chip information or simplifying the far-field pattern acquisition process is a promising method for further performance optimization.

### 5. Future trends

Feedback photonic parameter tuning is essential to all integrated photonic systems with stability and dynamic operations requirements. We point out several future trends. First of all, most designs still use board-level solutions, and integrated solutions are required as the system scales up. Second, we can extend it to photonic devices with different materials and structures, e.g., thin-film lithium niobite (TFLN), indium phosphide (InP) devices. Third, it is vital to reduce the hardware cost while still obtaining sufficient monitoring information. Fourth, we can extend it to multi-dimensional cases that include different wavelengths, polarization, modes, etc. Fifth, we can specialize the proposed model to more applications, such as switches array, optical phased array, and optical neural network. Sixth, we can extend this model from classical photonics to quantum photonics. Seventh, PMC with a wide operating range and high scalability deserves further study,

and more advanced PMC architectures, such as hybrid power converters and dynamic power management, can be applied to this model. Eighth, the stability of the hybrid closed-loop system deserves further investigation. Ninth, it is important to characterize the non-ideal effects (e.g., thermal cross talk) on system performance and invent methods to mitigate them. Tenth, we can replace thermo-optical tuning with other tuning mechanisms, e.g., electro-acoustic-optical tuning, electro-optic tuning, or combine multiple tuning mechanisms. Finally, for performance optimization, a holistic approach is needed, and the co-design of all building blocks is essential.

## 6. Conclusion

The convergence of electronics and photonics is one of the key post-Moore's research directions. The rapid development of silicon photonics is accelerating this convergence process. Thermo-optic feedback tuning forms the foundation of any stable and dynamic silicon photonic system and is currently experiencing rapid development. As the convergence process continues, electronics and photonics will be converged at the circuit level and thermo-optic feedback tuning eventually will form the electronic-photonic-converged thermo-optic feedback tuning.

## Acknowledgements

This work was supported by the National Key Research and Development Program of China (No. 2018YFA0704400).

## References

- [1] Mashanovich G Z. Electronics and photonics united. *Nature*, 2018, 556, 316
- [2] Tan M, Ming D, Wang Z C. From photonic integration to electronic-photonic heterogeneously-converging integrated circuits: A case study of wavelength locking of microrings. *Micro/nano Electronics and Intelligent Manufacturing*, 2019, 1(3), 40 (in Chinese)
- [3] Shen Y, Harris N C, Skirlo S, et al. Deep learning with coherent nanophotonic circuits. *Nat Photonics*, 2017, 11, 441
- [4] Chung S, Abediasl H, Hashemi H. A monolithically integrated large-scale optical phased array in silicon-on-insulator CMOS. *IEEE J Solid-State Circuits*, 2018, 53, 275
- [5] Wang J, Paesani S, Ding Y, et al. Multidimensional quantum entanglement with large-scale integrated optics. *Science*, 2018, 360, 285
- [6] Malik A, Dwivedi S, Landschoot L V, et al. Ge-on-Si and Ge-on-SOI thermo-optic phase shifters for the mid-infrared. *Opt Express*, 2014, 22, 28479
- [7] Hashizume Y, Katayose S, Tsuchizawa T, et al. Low-power silicon thermo-optic switch with folded waveguide arms and suspended ridge structures. *Electron Lett*, 2012, 48, 1234
- [8] Qiu H, Liu Y, Luan C, et al. Energy-efficient thermo-optic silicon phase shifter with well-balanced overall performance. *Opt Lett*, 2020, 45, 4806
- [9] Miller S A, Chang Y C, Phare C T, et al. Large-scale optical phased array using a low-power multi-pass silicon photonic platform. *Optica*, 2020, 7, 3
- [10] Watts M R, Sun J, DeRose C, et al. Adiabatic thermo-optic Mach-Zehnder switch. *Opt Lett*, 2013, 38, 733
- [11] Campenhout J V, Green W M J, Assefa S, et al. Integrated NiSi waveguide heaters for CMOS-compatible silicon thermo-optic devices. *Opt Lett*, 2010, 35, 1013
- [12] Fang Q, Song J F, Liow T, et al. Ultralow power silicon photonics thermo-optic switch with suspended phase arms. *IEEE Photon Technol Lett*, 2011, 23, 525
- [13] Chung S, Nakai M, Hashemi H. Low-power thermo-optic silicon modulator for large-scale photonic integrated systems. *Opt Express*, 2019, 27, 13430
- [14] Jacques M, Samani A, El-Fiky E, et al. Optimization of thermo-optic phase-shifter design and mitigation of thermal crosstalk on the SOI platform. *Opt Express*, 2019, 27, 10456
- [15] Baets R, Baets R, Subramanian A Z, et al. Silicon photonics: Silicon nitride versus silicon-on-insulator. *Optical Fiber Communication Conference*, 2016, Th3J.1
- [16] Chen Y, Whitehead J, Ryou A, et al. A large thermal tuning of a polymer-embedded silicon nitride nanobeam cavity. *Opt Lett*, 2019, 44, 3058
- [17] Bauters J F, Heck M J R, John D, et al. Ultra-low-loss high-aspect-ratio Si<sub>3</sub>N<sub>4</sub> waveguides. *Opt Express*, 2011, 19, 3163
- [18] Hosseini E S, Yegnanarayanan S, Atabaki A H, et al. A high quality planar silicon nitride microdisk resonators for integrated photonics in the visible wavelength range. *Opt Express*, 2009, 17, 14543
- [19] Sun Y, Cao Y, Wang Q, et al. Polymer thermal optical switch for a flexible photonic circuit. *Appl Opt*, 2018, 57, 14
- [20] Liu Y F, Wang X B, Sun J W, et al. Improved performance of thermal-optic switch using polymer/silica hybrid and air trench waveguide structures. *Opt Lett*, 2015, 40, 1888
- [21] Masood A, Pantouvaki M, Lepage G, et al. Comparison of heater architectures for thermal control of silicon photonic circuits. *10th International Conference on Group IV Photonics*, 2013, 83
- [22] Ye K, Tan M. A dual-channel digital low dropout regulator with time-division-multiplexing scheme. *IEEE International Conference on Integrated Circuits, Technologies and Applications (ICTA)*, 2019, 29
- [23] Bahadori M, Gazman A, Janosik N, et al. Thermal rectification of integrated microheaters for microring resonators in silicon photonics platform. *J Light Technol*, 2018, 36, 773
- [24] Zecevic N, Hofbauer M, Zimmermann H. Integrated pulsewidth modulation control for a scalable optical switch matrix. *IEEE Photon J*, 2015, 7, 1
- [25] Zhu Q, Qiu C, He Y, et al. Self-homodyne wavelength locking of a silicon microring resonator. *Opt Express*, 2019, 27, 36625
- [26] Gatdula R, Kim K, Melikyan A, et al. Simultaneous four-channel thermal adaptation of polarization insensitive silicon photonics WDM receiver. *Opt Express*, 2017, 25, 27119
- [27] Hattink M, Zhu Z, Bergman K. Automated tuning and channel selection for cascaded micro-ring resonators. *Metro and Data Center Optical Networks and Short-Reach Links III*, 2020, 11308, 113080P
- [28] Agarwal S, Ingels M, Pantouvaki M, et al. Wavelength locking of a Si ring modulator using an integrated drop-port OMA monitoring circuit. *IEEE J Solid-State Circuits*, 2016, 51, 2328
- [29] Dong P, Gatdula R, Kim K, et al. Simultaneous wavelength locking of microring modulator array with a single monitoring signal. *Opt Express*, 2017, 25, 16040
- [30] AlTaha M W, Jayatilleka H, Lu Z, et al. Monitoring and automatic tuning and stabilization of a 2 × 2 MZI optical switch for large-scale WDM switch networks. *Opt Express*, 2019, 27, 24747
- [31] Saeedi S, Emami A. Silicon-photonic PTAT temperature sensor for micro-ring resonator thermal stabilization. *Opt Express*, 2015, 23, 21875
- [32] Yang S, Zhu X, Zhang Y, et al. Thermal stabilization of a microring resonator using bandgap temperature sensor. *IEEE Optical Interconnects Conference (OI)*, 2015, 44
- [33] Kim M, Kim M H, Jo Y, et al. A fully integrated 25 Gb/s Si ring modu-

- lator transmitter with a temperature controller. Optical Fiber Communication Conference, 2020, T3H.7
- [34] Jayatilika H, Murray K, Guillén-Torres M Á, et al. Wavelength tuning and stabilization of microring-based filters using silicon in-resonator photoconductive heaters. *Opt Express*, 2015, 23, 25084
- [35] Jayatilika H, Shoman H, Boeck R, et al. Automatic configuration and wavelength locking of coupled silicon ring resonators. *J Lightwave Technol*, 2018, 36, 210
- [36] Jayatilika H, Shoman H, Chrostowski L, et al. High quantum efficiency photoconductive heaters enable control of large-scale silicon photonic ring resonator circuits. *Optica*, 2019, 6, 84
- [37] Morichetti F, Grillanda S, Carminati M, et al. A non-invasive on-chip light observation by contactless waveguide conductivity monitoring. *IEEE J Sel Top Quantum Electron*, 2014, 20, 292
- [38] Zanetto F, Grimaldi V, Moralis-Pegios M, et al. A WDM-based silicon photonic multi-socket interconnect architecture with automated wavelength and thermal drift compensation. *J Lightwave Technol*, 2020, 38, 6000
- [39] Grillanda S, Carminati M, Morichetti F, et al. A non-invasive monitoring and control in silicon photonics using CMOS integrated electronics. *Optica*, 2014, 1, 129
- [40] Zhu Q, Jiang X, Yu Y, et al. Automated wavelength alignment in a  $4 \times 4$  silicon thermo-optic switch based on dual-ring resonators. *IEEE Photon J*, 2018, 10, 1
- [41] Guglielmi E, Carminati M, Zanetto F, et al. 16-channel modular platform for automatic control and reconfiguration of complex photonic circuits. IEEE International Symposium on Circuits and Systems (ISCAS), 2017, 1
- [42] Moralis-Pegios M, Pitris S, Alexoudi T, et al. 4-channel 200 Gb/s WDM O-band silicon photonic transceiver sub-assembly. *Opt Express*, 2020, 28, 5706
- [43] Kim M H, Zimmermann L, Choi W Y. A temperature controller IC for maximizing Si micro-ring modulator optical modulation amplitude. *J Lightwave Technol*, 2019, 37, 1200
- [44] Li C, Bai R, Shafik A, et al. Silicon photonic transceiver circuits with microring resonator bias-based wavelength stabilization in 65 nm CMOS. *IEEE J Solid-State Circuits*, 2014, 49, 1419
- [45] Li H, Xuan Z, Titriku A, et al. A 25 Gb/s, 4.4 V-swing, AC-coupled ring modulator-based WDM transmitter with wavelength stabilization in 65 nm CMOS. *IEEE J Solid-State Circuits*, 2015, 50, 3145
- [46] Sun C, Wade M, Georgas M, et al. A 45 nm CMOS-SOI monolithic photonics platform with bit-statistics-based resonant microring thermal tuning. *IEEE J Solid-State Circuits*, 2016, 51, 893
- [47] Yu K, Li C, Li H, et al. A 25 Gb/s hybrid-integrated silicon photonic source-synchronous receiver with microring wavelength stabilization. *IEEE J Solid-State Circuits*, 2016, 51, 2129
- [48] Padmaraju K, Logan D F, Shiraishi T, et al. Wavelength locking and thermally stabilizing microring resonators using dithering signals. *J Light Technol*, 2014, 32, 505
- [49] Annoni A, Guglielmi E, Carminati M, et al. Automated routing and control of silicon photonic switch fabrics. *IEEE J Sel Top Quantum Electron*, 2016, 22, 169
- [50] Wang L L, Kowalczyk T. A versatile bias control technique for any-point locking in lithium niobate Mach-Zehnder modulators. *J Light Technol*, 2010, 28, 1703
- [51] Wang Z, Yu Y, Xiao X, et al. A time-division-multiplexing scheme for simultaneous wavelength locking of multiple silicon microrings. IEEE International Symposium on Circuits and Systems (ISCAS), 2018, 1
- [52] Mak J C C, Sacher W D, Xue T, et al. Automatic resonance alignment of high-order microring filters. *IEEE J Quantum Electron*, 2015, 51, 1
- [53] Milanizadeh M, Aguiar D, Melloni A, et al. Canceling thermal cross-talk effects in photonic integrated circuits. *J Light Technol*, 2019, 37, 1325
- [54] Milanizadeh M, Ahmadi S, Petrini M, et al. Control and calibration recipes for photonic integrated circuits. *IEEE J Sel Top Quantum Electron*, 2020, 26, 1
- [55] Ming D, Wang C, Wang Y, et al. First demonstration of closed-loop PWM wavelength locking of a microring resonator in a monolithic photonic-BiCMOS platform. IEEE International Conference on Integrated Circuits, Technologies and Applications (ICTA), 2020
- [56] Padmaraju K, Logan D F, Zhu X, et al. Integrated thermal stabilization of a microring modulator. *Opt Express*, 2013, 21, 14342
- [57] Li H, Balamurugan G, Kim T, Sakib M N, et al. A 3-D-integrated silicon photonic microring-based 112-Gb/s PAM-4 transmitter with nonlinear equalization and thermal control. *IEEE J Solid-State Circuits*, 2020, 1
- [58] Amberg P, Chang E, Liu F, et al. A sub-400 fJ/bit thermal tuner for optical resonant ring modulators in 40 nm CMOS. IEEE Asian Solid State Circuits Conference (A-SSCC), 2012, 29
- [59] Tan M. A precoding closed-loop feedback thermal control method and system for microring modulator. Chinese Patent, 2017, 201711029849.1 (in Chinese)
- [60] Nagata H, Kiuchi K, Saito T. Studies of thermal drift as a source of output instabilities in Ti:LiNbO<sub>3</sub> optical modulators. *J Appl Phys*, 1994, 75, 4762
- [61] Wooten E L, Kissa K M, Yi-Yan A, et al. A review of lithium niobate modulators for fiber-optic communications systems. *IEEE J Sel Top Quantum Electron*, 2000, 6, 69
- [62] Chen H, Zhang B, Ma W, et al. Study on auto bias control of a silicon optical modulator in a four-level pulse amplitude modulation format. *Appl Opt*, 2019, 58, 3986
- [63] Švarný J. Limited applicability of the constant optical power controller to the integrated intensity electro-optic modulator. Proc 10th World Scientific Engineering Academy Society, 2011, 108
- [64] Švarný J. Analysis of quadrature bias-point drift of Mach-Zehnder electro-optic modulator. 12th Biennial Baltic Electronics Conference, 2010, 231
- [65] Fu Y, Zhang X, Hraimel B, et al. Mach-Zehnder: A review of bias control techniques for Mach-Zehnder modulators in photonic analog links. *IEEE Microw Mag*, 2013, 14, 102
- [66] Kim M H, Jung H Y, Zimmermann L. An integrated Mach-Zehnder modulator bias controller based on eye-amplitude monitoring. Smart Photonic and Optoelectronic Integrated Circuits XVIII, 2016, 9751, 97510X
- [67] Kim M, Yu B, Choi W. A Mach-Zehnder modulator bias controller based on OMA and average power monitoring. *IEEE Photon Technol Lett*, 2017, 29, 2043
- [68] Barwicz T, Watts M R, Popović M A, et al. Polarization-transparent microphotonic devices in the strong confinement limit. *Nat Photonics*, 2007, 1, 57
- [69] Caspers J N, Wang Y, Chrostowski L, et al. Active polarization independent coupling to silicon photonics circuit. Silicon Photonics and Photonic Integrated Circuits IV, 2014, 9133, 91330G
- [70] Velha P, Soriano V, Preite M V, et al. Wide-band polarization controller for Si photonic integrated circuits. *Opt Lett*, 2016, 41, 5656
- [71] Ma M, Murray K, Ye M, et al. Silicon photonic polarization receiver with automated stabilization for arbitrary input polarizations. Conference on Lasers and Electro-Optics, 2016, STu4G.8
- [72] Cao R, He Y, Zhu Q, et al. Multi-channel 28-GHz millimeter-wave signal generation on a silicon photonic chip with automated polarization control. *J Semicond*, 2019, 40, 052301
- [73] Ma M, Shoman H, Tang K, et al. Automated control algorithms for silicon photonic polarization receiver. *Opt Express*, 2020, 28, 1885

- [74] Ma M, Shoman H, Shekhar S, et al. Automated adaptation and stabilization of a tunable WDM polarization-independent receiver on active silicon photonic platform. *IEEE Photon J*, 2020, 12, 4900411
- [75] Sun S, He M, Xu M, et al. Bias-drift-free Mach-Zehnder modulators based on heterogeneous silicon and lithium niobate platform. *Photonics Res*, 2020, 8, 1958
- [76] Fatemi R, Khachaturian A, Hajimiri A. A nonuniform sparse 2-D large-FOV optical phased array with a low-power PWM drive. *IEEE J Solid-State Circuits*, 2019, 54, 1200
- [77] Kim T, Bhargava P, Poulton C V, et al. A single-chip optical phased array in a wafer-scale silicon photonics /CMOS 3D-integration platform. *IEEE J Solid-State Circuits*, 2019, 54, 3061
- [78] Ashtiani F, Aflatouni F. N x N optical phased array with 2N phase shifters. *Opt Express*, 2019, 27, 27183
- [79] Ashtiani F, Aflatouni F. Monolithic optical phased-array transceiver in a standard SOI CMOS process. *Opt Express*, 2015, 23, 6509
- [80] Zhang Q, Zhang L, Li Z, et al. An antenna array initial condition calibration method for integrated optical phased array. *Acta Photonica Sinica*, 2020, 49(7), 726001
- [81] Hutchisonetal D, Sun J, Doyle J, et al. High-resolution aliasing-free optical beam steering. *Optica*, 2016, 8, 887
- [82] Zhang H, Zhang Z, Peng C, et al. Phase calibration of on-chip optical phased arrays via interference technique. *IEEE Photon J*, 2020, 12, 6600210
- [83] Komljenovic T, Pintus P. On-chip calibration and control of optical phased arrays. *Opt Express*, 2018, 26, 3199



**Min Tan** received the Ph.D. degree from The Hong Kong University of Science and Technology in 2015. In 2016, he joined the Huazhong University of Science and Technology, where he is currently a Professor with the School of Electronic and Optical Information. His current research interests include circuit-level convergence of electronics and photonics.